Interaction between a bisphosphonate, tiludronate and nanocrystalline apatite: *in vitro* viability and proliferation of HOP and HBMSC cells

P Pascaud[1], **R Bareille**[2,3], **C Bourget**[2,3], **J Amédée**[2,3], **C Rey**[1] **and S Sarda**[1]

[1] CIRIMAT Carnot Institute, Université de Toulouse,CNRS/INPT/UPS, ENSIACET, 4 Allée Emile Monso, BP 44362, 31030 Toulouse Cedex 04, France
[2] Inserm U1026, Bioingénierie Tissulaire, 33076 Bordeaux Cedex, France
[3] Université Bordeaux Segalen, 33076 Bordeaux Cedex, France

E-mail: stephanie.sarda@iut-tlse3.fr

Abstract

Nanocrystalline apatites (NCA) are the inorganic components of mineralized tissues and they have been recently proposed as biomaterials for drug delivery systems. Bisphosphonates (BPs) are currently the reference drugs used to treat diseases involving bone disorders such as osteoporosis. Nevertheless, the interaction phenomena between BP molecules and apatite nanocrystals of bone are not well understood. Therefore, the adsorption characteristics have been examined and cellular activity of tiludronate molecules on NCA as models of bone mineral has been investigated. Adsorption experiments of tiludronate onto NCA were carried out and revealed a Langmuir-type adsorption isotherm. The uptake of tiludronate molecules is associated with a release of phosphate ions, indicating that the main reaction is an ion exchange process involving surface anions. The results evidence the strong affinity of BP molecules for the apatitic surface. The interactions of NCA–tiludronate associations with human osteoprogenitor cells and human bone marrow stromal cells do not reveal any cytotoxicity and evidence the activity of adsorbed tiludronate molecules. Moreover, an evolution of the physico-chemical characteristics of the apatitic substrate during biological study was observed, highlighting the existence of dynamic interactions. This work contributes to clarifying the reaction mechanisms between BPs and biomimetic apatites.

1. Introduction

Although calcium phosphate stoichiometric hydroxyapatite $Ca_{10}(PO_4)_6(OH)_2$ is frequently considered as a model compound for biological mineralization, the most relevant model concerning bone minerals is certainly that of non-stoichiometric calcium phosphate nanocrystalline apatites (NCAs) exhibiting the general formula (Montel *et al* 1981)

$$Ca_{10-x}(PO_4)_{6-x}(HPO_4^{2-} \text{or } CO_3^{2-})_x(OH)_{2-x} \quad \text{with} \quad 0 \leqslant x \leqslant 2. \tag{1}$$

These nanocrystals exhibit a special feature as shown in previous investigations using spectroscopic techniques (Rey *et al* 2007a). Recently, precipitated nanocrystals possessed a prominent structured hydrated layer on their surfaces, which is gradually converted into more stable apatite domains during ageing. This hydrated layer contains mineral ions in 'non-apatitic' environments which are easy to exchange and substitute reversibly by other ions in aqueous solutions. The adsorption properties of nanocrystals depend on the hydrated layer composition and the extent of this layer relates to the maturation stage of the nanocrystals. Biomimetic NCA are

used as bioactive biominerals for orthopaedic applications (Rey *et al* 2007b) and have been recently proposed as biomaterials for drug delivery systems (Autefage *et al* 2009, Palazzo *et al* 2007).

Bone is a dynamic tissue which undergoes a continuous rebuilding process during life as a result of the coupled actions of bone cells: osteoclasts promote resorption of old tissue while osteoblasts initiate new tissue formation (Eriksen *et al* 2007, Brandi and Collin-Osdoby 2006). However the equilibrium between bone resorption and formation differs in different phases of life and is strongly affected by bone diseases, such as osteoporosis, Paget's disease and hypercalcemia (Meunier 2005, Rodan and Fleisch 1996). Bisphosphonates (BPs) are currently the most prescribed drugs for the treatment of diseases involving bone turn-over disorders (Leu *et al* 2006, Russell *et al* 2008). BPs were first studied over 30 years ago as substitutes for inorganic pyrophosphate; they are characterized by a non-hydrolysable P–C–P structure with two phosphonic acid groups bonded to the same carbon. Their mechanisms of action are due to the conjunction of physicochemical effects and biological activity; like pyrophosphate, BPs present a high affinity to adsorb onto apatite crystals, and they have been shown to prevent mineral dissolution. In addition, they inhibit osteoclast activity and bone resorption (Russell and Rogers 1999, Leu *et al* 2006).

The classic BP treatment is the systemic way of oral administration or intravenous injection. However, systemic use of BPs can result in undesirable side effects (Coleman *et al* 2011) such as fever (Mönkkönen *et al* 1998), gastrointestinal disturbances such as ulcers (Elliott *et al* 1997) or osteonecrosis of the jaw, especially observed with intravenous preparations (Kos and Luczak 2009). Moreover a low bioavailability is commonly observed for oral administration (Hoffman *et al* 2001). On this basis, the development of strategies for local administration of BPs at bone sites exhibiting a risk of fracture (vertebra, hip, wrist, etc) becomes even more interesting. In the literature, BPs have been associated with calcium phosphate ceramics (Denissen *et al* 1994, Josse *et al* 2005), cements (Panzavolta *et al* 2009) or hydroxyapatite (McLeod *et al* 2006, Boanini *et al* 2007, Errassifi *et al* 2010, Nancollas *et al* 2006) and rarely adsorbed onto NCAs (Errassifi *et al* 2009, 2010, Palazzo *et al* 2007), though they mimic bone mineral more precisely than stoichiometric hydroxyapatite generally used. The aim of this work was to clarify the reaction mechanisms between a BP molecule, tiludronate and a biomimetic apatite.

Moreover, with the main action of BPs being their inhibitory effects on osteoclasts (Fleisch 2000, Russell *et al* 2008), very few studies have indeed examined the direct action of adsorbed BPs on osteoblasts (Panzavolta *et al* 2009, Boanini *et al* 2007). Although the activities of these cells are strongly linked (Fleisch 2000), suggesting indirect effects, the direct interaction between BPs and osteoblasts cells, or more generally osteoblast precursors, has never been appraised using the nanocrystalline apatitic model, and must be therefore explored. In this work, we investigated more precisely the interaction of NCA/tiludronate associations on pre-osteoblastic cells.

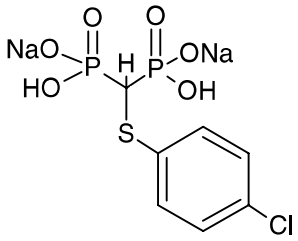

Figure 1. Molecular structure of tiludronate.

2. Materials and methods

2.1. Materials

A NCA powder close to mature bone mineral composition was synthesized by the double decomposition technique at ambient temperature and physiological pH (Rey *et al* 1989, 1995). NCA was prepared by pouring a calcium solution ($Ca(NO_3).4H_2O$, $C = 69.6$ g L^{-1}, in 750 mL) into a carbonate phosphate solution ($(NH_4)_2HPO_4$, $C = 80$ g L^{-1}, and $NaHCO_3$, $C = 60$ g L^{-1}, in 1500 mL). The precipitate obtained was left to mature for one month at room temperature. Subsequently, NCA was quickly vacuum-filtered, washed with deionised water and freeze-dried. The powder was then sieved (<125 μm) and stored in a freezer.

Powder of tiludronate (di-sodium((4-chlorophenyl) thio)methylene-bis-phosphonate) hemihydrate (figure 1) was a gift from Sanofi Aventis (France).

2.2. Adsorption

2.2.1. Sample preparation. In a polyethylene tube, 50 mg of poorly crystalline apatite powders were dispersed in 5 mL of an adsorption medium, an aqueous solution of tiludronate at different concentrations: 0, 0.5, 1, 1.5, 2 and 2.5 g L^{-1} in KCl (1 mM) (Errassifi *et al* 2009, Al-Kattan *et al* 2010). Then pH was adjusted at physiological pH by addition of KOH and HCl solutions. The suspensions obtained were sonicated for a few minutes and incubated for 2 h at physiological temperature (37 °C) without stirring to reach an adsorption equilibrium, then centrifuged for 20 min (at 5000 rpm). The supernatants were filtered onto Millipore (0.2 μm) before chemical analyses. The powder was washed once with 5 mL of deionized water and freeze-dried, and stored in a freezer. It has been checked that a second washing with the same amount of water removed only a negligible amount of tiludronate.

2.2.2. Characterization techniques. The phosphate content of synthesized apatite sample was determined by spectrometry of the phosphovanadomolybdic acid complex (Charlot 1974). The calcium content was determined by complexometry with ethylenediaminetetraacetic acid (EDTA). The specific surface area of the sample was evaluated using the Brunauer–Emmett–Teller method (nitrogen adsorption) on a Quantachrome Instruments Monosorb Nova 1000. The average size of NCA aggregates d (0.5) was obtained using a laser granulometer (Malvern Mastersizer 2000). The amount of carbonate ions of the apatite powder was measured by coulometry

techniques (UIC, Inc. CM 5014 coulometer with CM 5130 acidification unit). The solid phase was identified by x-ray diffraction (XRD) (Seifert XRD-3000TT diffractometer, CuKα1 radiation with $\lambda = 1.5406$ Å).

The characterization of the powders after adsorption was performed by different spectroscopic methods such as Fourier-transform infrared (FTIR), solid-state NMR and Raman microspectroscopy. FTIR experiments were performed on a Thermo Nicolet 5700 FTIR spectrometer using the KBr pellet method (2 mg sample/300 mg KBr); spectra were recorded in the 4000–400 cm^{-1} range, at 64 scans accumulation and 4 cm^{-1} resolution. Solid-state NMR experiments were recorded on a Bruker Avance 400 spectrometer equipped with a 4 mm probe. Samples were spun at 8 kHz at the magic angle using ZrO_2 rotors. For ^{31}P MAS single-pulse experiments, small flip angles ($\sim 30°$) were used with recycle delays of 20 s and with high-power proton decoupling conditions. ^{31}P chemical shifts were referenced to an external 85% H_3PO_4 sample. Raman microspectroscopy analysis was carried out using a Horiba, Jobin Yvon Labram HR800 confocal microspectrometer, equipped with a helium–neon laser ($\lambda = 632.82$ nm), over a wavenumber range of 350–1750 cm^{-1}.

The tiludronate concentration in the solution was determined by UV adsorption spectroscopy at 265 nm (single beam UV/Vis Hitachi U-1100 spectrophotometer). The amount of calcium and phosphate ions released upon adsorption was measured respectively by inductively coupled plasma atomic emission spectroscopy (Horiba, Jobin Yvon, 2004, Ultima 2, ICP-AES) and by spectrometry of the phosphovanadomolybdic acid complex.

2.3. Biological analyses

2.3.1. Sample preparation. For the substrates used in cell culture experiments, a large quantity of NCA with tiludronate was prepared by dispersing 0.5 g of apatite powder in 50 mL of adsorption medium (2 g L^{-1} of tiludronate, 1 mM KCl) using experimental process previously described. The equilibrium concentration was about 1.57 mM. Several powder lots were mixed to obtain a homogenous sample. Subsequently the powders were pressed by uniaxial pressing to form pellets (diameter 1 cm, weight 50 mg, at 190 MPa at room temperature) of NCA with and without BPs.

2.3.2. Isolation and culture of HBMSCs and HOPs. HBMSCs were obtained according to Vilamitjana-Amedee *et al* (1993), with some modifications. Human bone marrow was aspired during hip prosthesis surgery from the iliac crest of healthy donors aged between 20 and 50 years, in accordance with the French ethics committee. Cells were separated and counted. Sequential passages through syringes fitted with 16-, 18- or 21-gauge needles into a single suspension were the technique used to separate the cells. The suspension thus obtained was split into two samples, centrifuged for 15 min at 800 rpm and only one was resuspended in the Iscove Modified Dulbecco's Medium (IMDM, Gibco, Invitrogen) supplemented with 10% (v/v) foetal calf serum (FCS, PAA) and 10^{-8} M dexamethasone (Sigma, St. Louis, MO, USA) in order to induce osteoblastic differentiation of adherent cells (Vilamitjana-Amedee *et al* 1993). These cells, called human osteoprogenitor cells (HOPs), express cbfa1/Runx2, ALP and type I collagen. Subculturing was carried out using 0.2% (w/v) trypsin and 5 mM EDTA.

To maintain undifferentiated HBMSCs in a non-oriented lineage, the pellet was resuspended with an alpha minimal essential medium (αMEM), (Invitrogen), supplemented with 10% (v/v) FCS. Cells were plated into 75 cm^2 cell culture flasks (Falcon) at a density of 5×10^5 cells cm^{-2} and incubated in a humidified atmosphere of 95% air, 5% CO_2 at 37 °C. Subculturing was performed as previously described.

2.3.3. Cell viability and proliferation assays. Cell viability was determined with the live/dead viability/cytotoxicity kit (molecular probes), according to the manufacturer's protocol. Cell proliferation assays were carried out according to Mosmann's technique (Mosmann 1983). All assays were replicated four times for each condition tested. The positive control used for cell proliferation was tissue culture polystyrene (TCPs) of plastic culture dishes. The pellets of materials were put on an agarose layer (2% (v/v)), prepared in 0.1M phosphate buffered saline (PBS at pH 7.4), to prevent cell attachment to plastic dishes. Then cells were seeded and incubated overnight at 37 °C in the corresponding medium of each cell type. Thereafter, pellets were seeded with a density of 30×10^3 cells per cm^2, cultured in the IMDM for HOPs or in αMEM for HBMSCs supplemented with 10% (v/v) FCS and incubated at 37 °C in a humidified atmosphere. After 1, 3, 7, 15 and 21 days, the cell metabolic activity was measured by the MTT assay in order to quantify the cell growth. The MTT assay is an observation technique based on the ability of mitochondrial enzyme of viable cells to metabolize a water-soluble tetrazolium dye 3-(4,5-dimethylthiazol-2-yl)-2,5-diphenyl tetrazolium bromide into an insoluble formazan salt. The MTT solution was incubated at 37 °C for 3 h, removed and insoluble formazan crystals formed were dissolved in dimethylsulfoxide. Then, 100 μL of this solution was aspirated and poured into another 96-well plate to measure the absorbance at 540 nm. This technique was allowed to quantify directly the cell proliferation because the intensity of the staining solution obtained is proportional to cell proliferation. The scanning electron microscope (SEM) examination was performed using a Hitachi S-2500 SEM with a LaB6 filament on samples gold-coated beforehand, in order to observe the morphology of the cells seeded onto the surface of the materials and the formation of a cell layer.

3. Results and discussions

3.1. Powder characterization

The solids obtained exhibited XRD patterns (figure 2) characteristic of poorly crystalline apatitic calcium phosphates (Eichert *et al* 2009) and no additional crystalline solid phase was observed after tiludronate adsorption. Chemical analysis of NCA gave a CO_3^{2-} concentration of 5.1 ± 0.4% wt

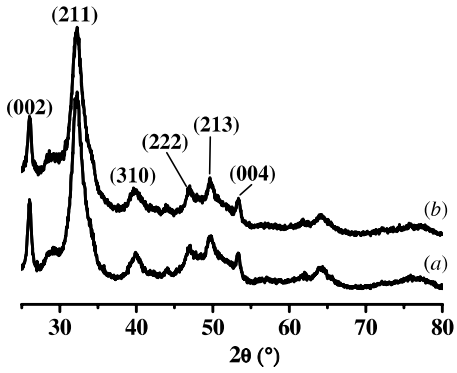

Figure 2. XRD diagrams for nanocrystalline apatite (NCA) powders before and after adsorption: (*a*) NCA and (*b*) NCA+BPs (equilibrium concentration at about 1.57 mM).

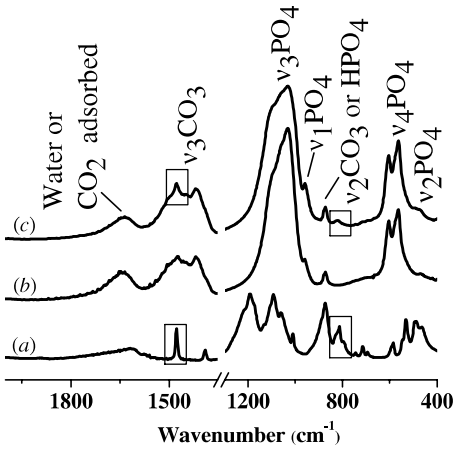

Figure 3. FTIR spectra for NCA powders before and after adsorption: (*a*) BPs, (*b*) NCA and (*c*) NCA+BPs (equilibrium concentration at about 1.57 mM).

(C/P ratio of 0.17) and Ca/P ratio of 1.61 characteristic of a calcium-deficient apatite (CDA). The specific surface area was evaluated to be 156 ± 9 m^2 g^{-1} and the average size of NCA aggregates $\underline{d}$ (0.5) was 31 μm. The nanocrystal size was determined by XRD using Scherrer's equation (Scherrer 1918): average length about 16.7 nm and average width thickness about 4.3 nm.

FTIR spectra of apatitic powders synthesized before adsorption (figure 3) showed characteristic vibration bands of poorly crystalline apatite: especially apatitic PO_4 bands at 469 (ν2), 562–603 (ν4), 962 (ν1) and 1000–1104 cm^{-1} (ν3) (Rey *et al* 2007a, Eichert *et al* 2009) and the apatitic HPO_4^{2-} band (550 cm^{-1}). Other vibration bands reveal the presence of non-apatitic environments of PO_4^{3-} (617 and 634 cm^{-1}) and HPO_4^{2-} (530 cm^{-1}) ions in the surface hydrated layer (Bohic *et al* 2000). This NCA model presents bands at 870, 1420 and 1470 cm^{-1} due to CO_3 vibrations characteristic of non-apatitic carbonates and type B carbonate species. The original tiludronate molecule presents several lines, particularly those associated with aromatic ring chains at 1480, 1500, 1580 and 1620 cm^{-1}, C–H and C–S vibrations at 1390 and 820 cm^{-1} and 710 cm^{-1}, respectively (Bonnery *et al* 1994). After adsorption, the spectrum of NCA displayed additional lines and shoulders characteristic of tiludronate

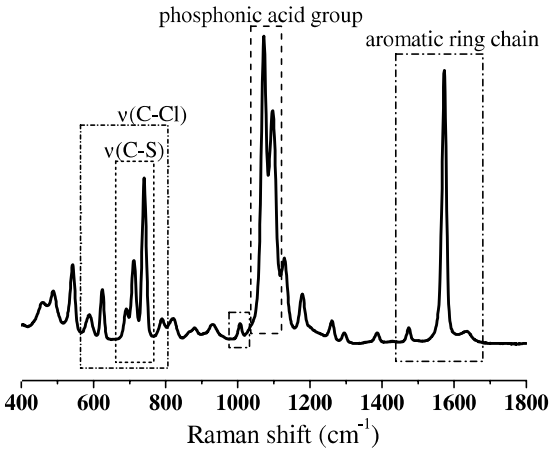

Figure 4. Raman spectrum of tiludronate.

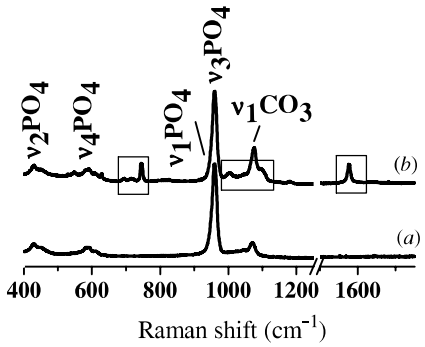

Figure 5. Raman spectra for NCA powders before and after adsorption: (*a*) NCA and (*b*) NCA+BPs (equilibrium concentration at about 1.57 mM).

Table 1. Raman bands observed for tiludronate.

Domain, Assignments	Raman (cm^{-1})
–	540
(Juillard *et al* 2010)	
ν(C–Cl)	550–800
ν(C–S) aliphatic	630–790
ν(C–S) aromatic	1080–1100
$\nu_{as}PO_3/\nu_{as}$ P–O(H)/δPO–H	1072, 1097
(Juillard *et al* 2010)	
ν (C–C) aromatic ring chain vibrations	1010, 1470, 1565, 1600

molecules at 1480 and 820 cm^{-1} , especially supporting the presence of a tiludronate on the precipitate.

The Raman spectroscopic study complemented FTIR data. The Raman spectrum of tiludronate (figure 4, table 1) exhibited four main regions: the first one between 550 and 800 cm^{-1} characteristic of ν(C–Cl) bands, the second one containing the ν(C–S) aliphatic bands in the 630–790 cm^{-1} region, the third one at 1072 and 1097 cm^{-1} corresponding to the two phosphonic acid groups and the last one is assigned to the aromatic ring chain at 1010, 1470, 1565 and 1600 cm^{-1} (Bonnery *et al* 1994, Wood 1930, Wood and Collins 1932). The Raman spectrum of powders obtained after adsorption (figure 5) showed the characteristic bands of the apatitic structure (Penel *et al* 1998), especially PO_4 bands at 469 (ν2), 562–603 (ν4), 962 (ν1)

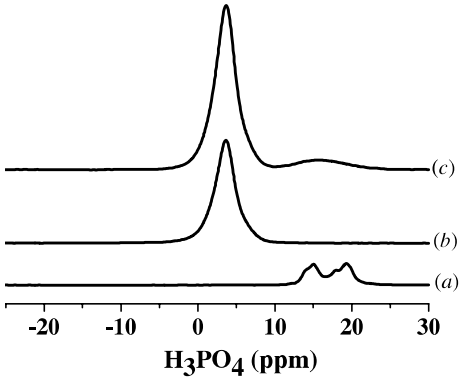

Figure 6. ^{31}P MAS NMR solid-state spectra for tiludronate: (*a*) BPs and for NCA powders before and after adsorption: (*b*) NCA and (*c*) NCA+BPs (equilibrium concentration at about 1.57 mM).

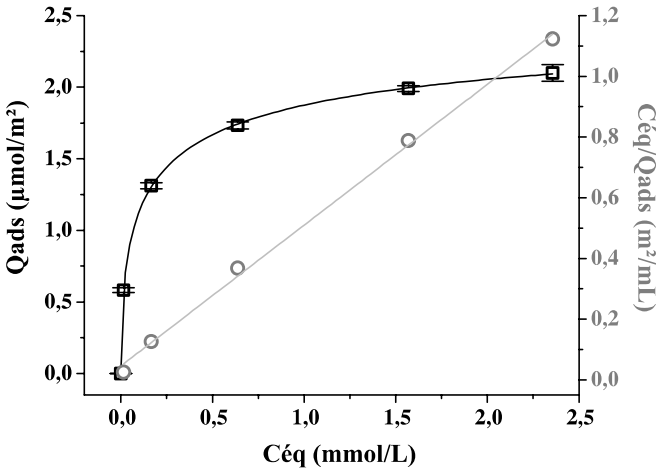

Figure 7. Adsorption isotherms of tiludronate by NCA from dilute aqueous solutions (□) and the corresponding linear regression of Langmuir (○).

and 1000–1104 cm^{-1} (ν3) (Rey *et al* 2007a, Eichert *et al* 2009) and CO_3^{2-} bands at 1070 cm^{-1}. Additional lines at 746 and 1575 cm^{-1} corresponding to C–S and aromatic ring chain vibrations of tiludronate can be assigned to tiludronate. Unfortunately, in FTIR and Raman spectra other lines of tiludronate, especially those of phosphonate groups, probably involved in the tiludronate/NCA association, are hidden by those of phosphate groups of NCA. In order to obtain more information on such interactions a solid-state NMR study was carried out.

The ^{31}P NMR spectra of tiludronate, NCA and tiludronate/NCA association are shown in figure 6. The spectrum of tiludronate shows two main lines at 15 and 19.3 ppm attributed to the ^{31}P nuclei of the two phosphonate groups of BPs, chemically non-equivalent (Errassifi *et al* 2009). The spectrum of NCA is characterized by a single asymmetric broad line at 3.3 ppm due to PO_4^{3-} and HPO_4^{2-} species (Eichert *et al* 2004). The spectrum of tiludronate/NCA association presents, in addition to the phosphate line of NCA, a weaker broad line at 15.7 ppm at about a chemical shift of phosphonate groups of tiludronate. Such broad lines have already been observed in a previous study by Mukherjee *et al* (2008) concerning the adsorption of several BPs bound to bone. The broadness of this line very different from that of tiludronate sodium salt suggests a lack of crystalline structure and seems in agreement with adsorbed BPs (Grossmann *et al* 2000).

3.2. Analyses of the solution

The evolution of the amount of tiludronate adsorbed from dilute solutions (0–6,7 mM) as a function of its remaining concentration in the solution is plotted in figure 7. The adsorption isotherms obtained are Langmuirian in shape in agreement with a previous study on another BP, risedronate (Errassifi *et al* 2010). The adsorption plateau was reached at relatively low equilibrium concentrations (about 1 mM) corresponding to a tiludronate load of 11wt%, highlighting the high affinity between tiludronate molecules and the NCA surface. Similar findings have been reported for the adsorption on NCA of biological macromolecules such as albumin, heparin, growth factors and risedronate molecules (Errassifi *et al* 2010). The affinity constant (K) and the amount adsorbed at saturation (N) were determined using a Langmuir linear regression (Langmuir 1918) as shown in figure 7:

$$\frac{C_{\mathrm{eq}}}{Q_{\mathrm{ads}}} = \frac{C_{\mathrm{eq}}}{N} + \frac{1}{(K \times N)} \qquad (2)$$

with C_{eq} (mmol L^{-1}) being the equilibrium concentration in the solution of tiludronate, Q_{ads} (μmol m^{-2}) the amount adsorbed per unit area, N (μmol m^{-2}) the amount adsorbed at saturation, K (L mmol^{-1}) the affinity constant of tiludronate for the NCA surface.

The values of K and N were respectively 10.14 $\pm$ 0.02 L mmol^{-1} and 2.17 $\pm$ 0.01 μmol m^{-2}. These values are close to the values previously obtained for the adsorption of risedronate molecules using similar experimental conditions (Errassifi 2011, Al-Kattan *et al* 2010). In addition, these studies have shown that higher amounts of BP adsorbed at saturation were obtained on NCA compared to well-crystallized stoichiometric hydroxyapatite. This phenomenon has been attributed to the presence of a surface hydrated layer on NCA offering more flexibility for molecule substitutions or incorporations than a patterned rigid mineral surface, like in a well-crystallized apatite. The affinity constant has been found to vary strongly depending on the nature of the adsorbing molecules (Nancollas *et al* 2006) and NCA surface characteristics (Ouizat *et al* 1999). The values obtained here confirm the high affinity of tiludronate for the NCA surface.

The calcium ion concentration in the solution was very low and weakly altered by the adsorption reaction (data not shown). It has been assumed to be mainly related to apatite dissolution equilibrium (Errassifi *et al* 2010, Al-Kattan *et al* 2010). A correlation exists between phosphate released in the solution and tiludronate adsorbed by the NCA surface (figure 8). In fact, the uptake of tiludronate is proportional to the amount of phosphate ions released in the solution (slope of 1.3 $\pm$ 0.1). Thereby, the adsorption of tiludronate onto NCA seems to be a chemisorption process corresponding to

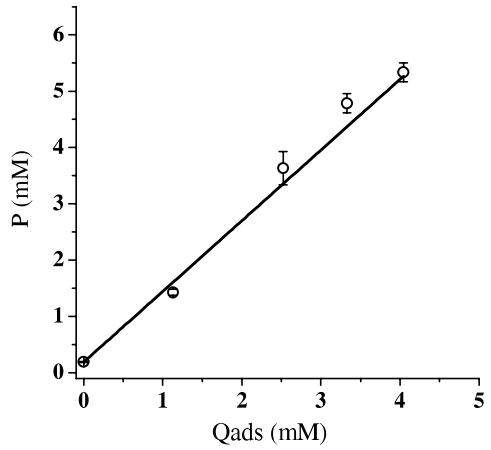

Figure 8. Concentration of phosphate ions in supernatants upon adsorption of tiludronate on NCA in 1 mM KCl solution at pH 7.4 and $T = 37$ °C.

an ion exchange between PO_3 anionic ends of tiludronate molecules in the solution and phosphate species from the NCA surface and/or carbonates. This phosphate exchange has already been observed for risedronate adsorbed onto NCA and hydroxyapatite by Errassifi *et al* (2009) and for zoledronate bound to βTCP and CDA by Roussière *et al* (2008). For example, the study of the adsorption of risedronate molecules onto hydroxyapatite showed an exchange process with close to the one-to-one substitution process (Al-Kattan *et al* 2010, Errassifi 2011). The exchange ratio appears different here and could depend on the composition of the hydrated layer, on the speciation of BP ions at the surface and, probably on the surface zeta potential variations. Other explanations could be proposed for the release of phosphate ions and Josse *et al* (2005), for example, have shown that for zoledronate interaction with calcium phosphate compounds, at high BP concentrations, crystalline calcium zoledronate needles were formed corresponding to a dissolution–reprecipitation mechanism. However, in our case, no foreign phase formation was detected. In addition, it shall be noted that in the case of dissolution–reprecipitation, a Langmuir isotherm would not have been obtained (Errassifi *et al* 2010).

3.3. Cell viability and differentiation

Live/dead assays performed on cellularized materials revealed that cells kept their viability over the time of cell culture (figure 9). This is corroborated by SEM examination (figure 10). These results highlight the absence of cytotoxicity of NCA, whatever the cell types. Cells kept their viability with time of culture onto these functionalized materials. Moreover, the morphology of the cells on pellets containing tiludronate evidences the absence of cytotoxicity of the drug at the concentration used. Cells remain spread on the materials and exhibit filipodia. These qualitative data were confirmed by the quantitative analysis and cell proliferation study.

Our results indicated that HOPs and HBMSCs exhibit similar kinetics of cell proliferation on both types of scaffolds (figure 11). Based on the MTT assay, tiludronate stimulated cellular proliferation whatever the nature of the cells (figure 11). The effect of tiludronate is evidenced on the two cell types throughout the culture time, from D1 to D21. Here, these results give evidence of tiludronate actions on undifferentiated cells, i.e. HBMSCs as was demonstrated for MG63, an osteoblastic cell line (Panzavolta *et al* 2009, Boanini *et al* 2008) and for human trabecular differentiated bone cells (Im *et al* 2004) with different BPs. In addition,

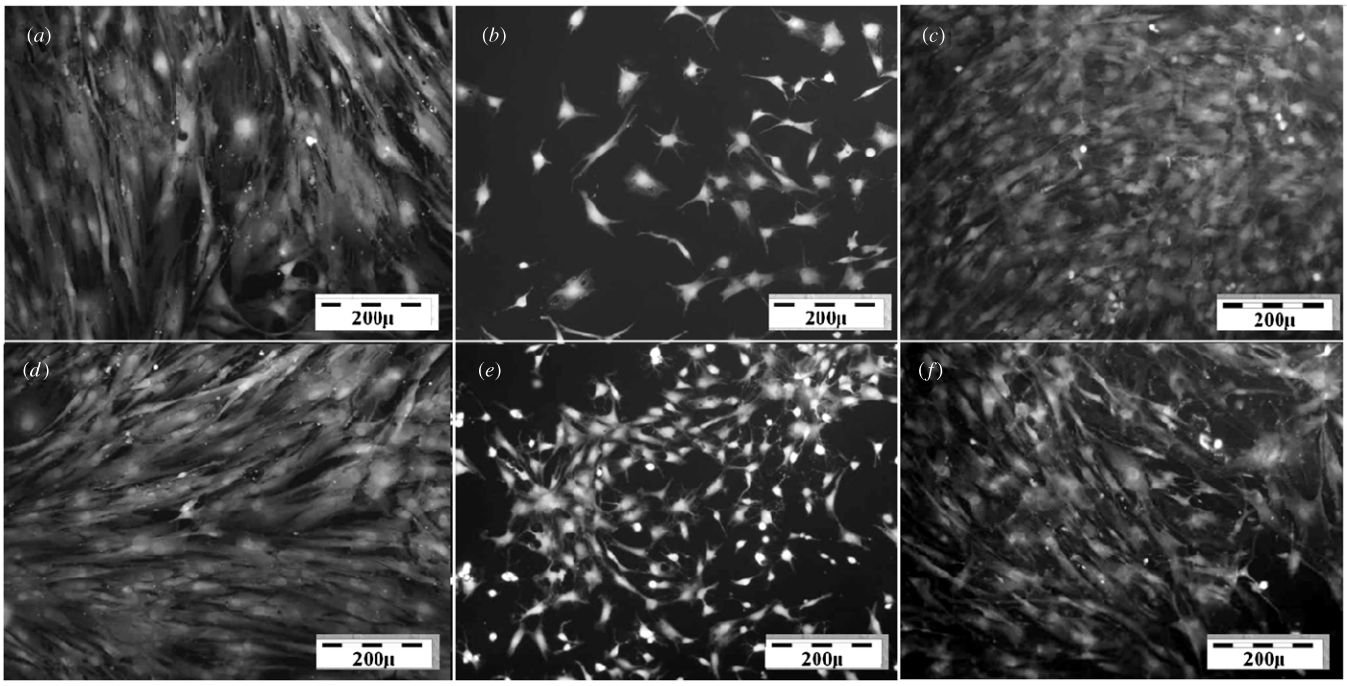

Figure 9. Live/dead assays performed on HOPs (*a*), (*b*), (*c*) and HMBSCs (*d*), (*e*), (*f*) cultured for 21 days on TCPs (*a*), (*d*), on NCA (*b*), (*e*) and on NCA+BP (*c*), (*f*) materials.

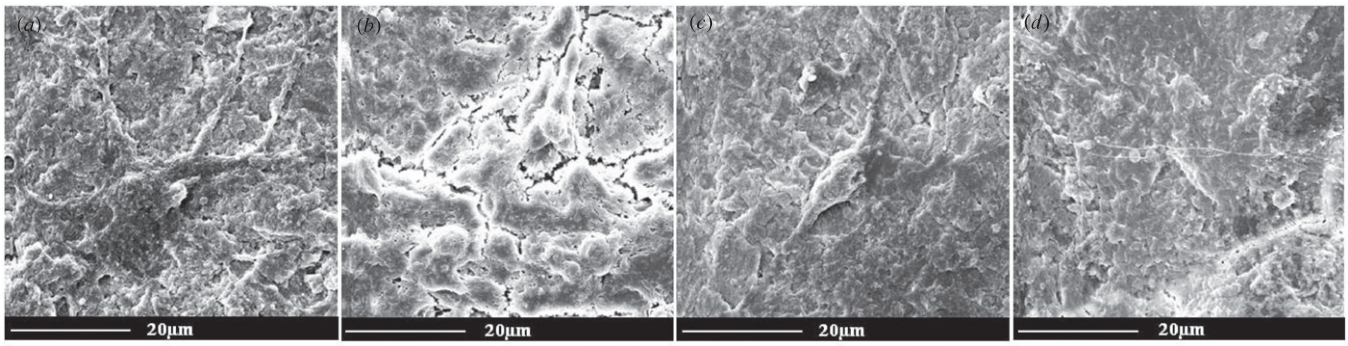

Figure 10. Scanning electron microscopy performed on HOPs (*a*),(*b*) and HMBSCs (*c*), (*d*), cultured for 21 days on NCA (*a*), (*c*) and NCA+BP (*b*), (*d*) materials.

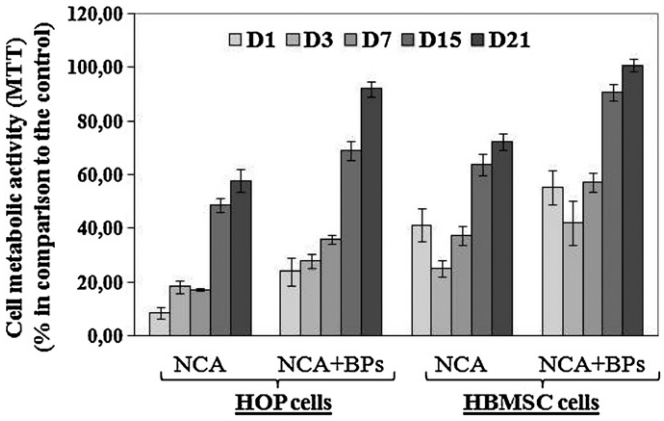

Figure 11. Cell proliferation of HOPs and HBMSCs on NCA and NCA+BP materials.

these data confirmed qualitative results obtained after 21 days (figures 9 and 10) showing spreading cells on NCA+BPs and the formation of a cell layer on these substrates.

3.4. Characterization of the pellets after cells experiments

As supports used for osteoblastic tests were non-stoichiometric poorly crystallized apatites, a physico-chemical evolution of nanocrystals towards more crystalline stoichiometric structure was expected in the aqueous solution (Rey *et al* 2007b). The pellets were analysed after cell experiments by FTIR spectroscopy. In the ν_4 PO_4 region, five main bands were detected for poorly crystalline synthetic apatite samples (Eichert *et al* 2009), as in bone mineral (Bohic 2000): a shoulder at 617 cm^{-1} assigned to labile phosphate groups, three bands at 600, 575 and 560 cm^{-1} due to phosphate ions in an apatitic environment and a shoulder at 533 cm^{-1} to non-apatitic HPO_4 ion vibration, as explained previously. Curve fitting was done with the GRAMS/386 program (Galactic Industries, Salem, NH), fixing or varying parameters (position and width of apatitic and non-apatitic bands) to provide the best curve fit. The band shape was considered Lorentzian in all instances and the baseline was always linear. The relative band integrated intensities were defined as the ratio of peak area to total area of the phosphate bands. Figure 12 reports the relative band integrated intensity for labile PO_4 and HPO_4 ions. These values decreased for non-apatitic HPO_4 ions with cell test times from 0 to 21 days, whatever the type of cells. These results are in agreement with the observed evolution of NCA with maturation time in the solution (Eichert *et al* 2009). Although such modifications of the surface composition probably have an effect on molecule adsorption and cell behaviour, this point has to be further investigated.

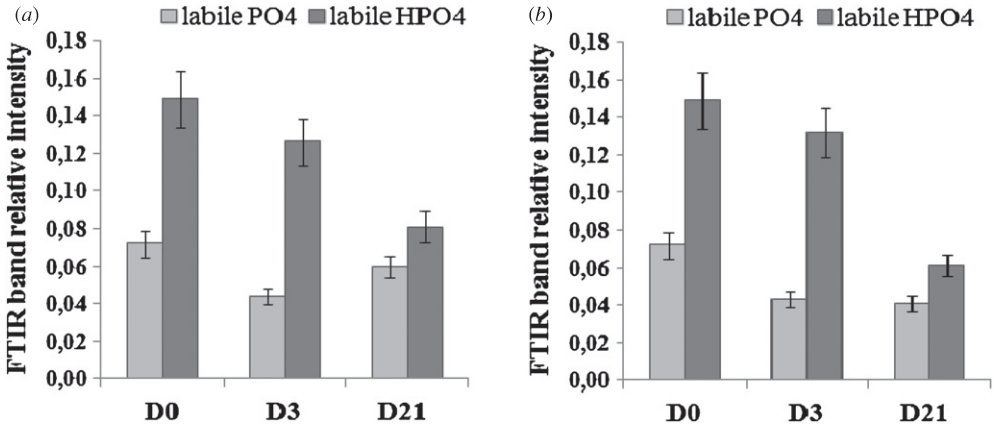

Figure 12. Evolution of labile PO_4^{3-} and HPO_4^{2-} contents with different time in culture medium: time 0 (D0); 3 days (D3) and 21 days (D21) with HOP (*a*) and HBMSC (*b*) cells for NCA, as determined by FTIR spectroscopy.

4. Conclusion

This work contributes to clarify the reaction mechanisms between tiludronate and biomimetic apatites. The adsorption characteristics were examined and the results obtained highlight the strong affinity of bisphosphonate (BP) molecules for the NCA surface. Spectroscopic techniques on solids such as the FTIR and Raman appear to be relevant methods to demonstrate molecular adsorption. Generally, adsorption studies of bone-bonding bioactive molecules or drugs are performed on well-crystallized hydroxyapatite and this work proposes models of bone nanocrystals with controlled physico-chemical characteristics and surface properties, allowing the screening of drugs in repeatable conditions closer to the biological situation. Whereas most papers investigate cell activity of BPs in the solution (Von Knoch *et al* 2005, Im *et al* 2004, Fromigue and Body 2002), our data clearly show that adsorbed molecules like tiludronate exhibit a biological effect, specifically a stimulation of cell proliferation of both cell types used in this work, HOPs and HBMSCs. Such findings appear important for the development and applications of drug delivery systems based on apatite nanocrystals and they have to be considered in bone mineral interactions with drugs. In further studies, the influence of these NCA characteristics (composition, crystallinity, etc) and thus the nature of the models used on the adsorption properties and cells response must be investigated.

Acknowledgments

The authors thank Sanofi Aventis for generously providing tiludronate (di-sodium((4-chlorophenyl)thio)methylene-bis-phosphonate) hemihydrate sample. This work was supported by AAP CNRS 2009 project 'Longévité et Vieillissement'.

References

Al-Kattan A *et al* 2010 Medical potentialities of biomimetic apatites through adsorption, ionic substitution, and mineral/organic associations: three illustrative examples *Adv. Eng. Mater.* **12** B224–33

Autefage H, Briand-Mésange F, Cazalbou S, Drouet C, Fourmy D, Gonçalvès S, Salles J-P, Combes C, Swider P and Rey C 2009 Adsorption and release of BMP-2 on nanocrystalline apatite-coated and uncoated hydroxyapatite/β-tricalcium phosphate porous ceramics *J. Biomed. Mater. Res.* B **91** 706–15

Boanini E, Gazzano M, Rubini K and Bigi A 2007 Composite nanocrystals provide new insight on alendronate interaction with hydroxyapatite structure *Adv. Mater.* **19** 2499–502

Boanini E, Torricelli P, Gazzano M, Giardino R and Bigi A 2008 Alendronate-hydroxyapatite nanocomposites and their interaction with osteoclasts and osteoblast-like cells *Biomaterials* **29** 790–6

Bohic S, Rey C, Legrand A, Sfihi H, Rohanizadeh R, Martel C, Barbier A and Daculsi G 2000 Characterization of the trabecular rat bone mineral: effect of ovariectomy and bisphosphonate treatment *Bone* **26** 341–8

Bonnery M, Bouisset M and Sole R 1994 Monohydrate of the disodium salt of 4-chlorophenylthiomethylene-bisphosphonic acid, its preparation and pharmaceutical compositions containing it *EP Patent* 0582515

Brandi M L and Collin-Osdoby P 2006 Vascular biology and the skeleton *J. Bone Miner. Res.* **21** 183–92

Charlot G 1974 *Chimie Analytique Quantitative* (Paris: Masson)

Coleman R, Burkinshaw R, Winter M, Neville-Webbe H, Lester J, Woodward E and Brown J 2011 Zoledronic acid *Expert Opin. Drug Saf.* **10** 133–45

Denissen H, Van Beek E, Löwik C, Papapoulos S and Van Den Hooff A 1994 Ceramic hydroxyapatite implants for the release of bisphosphonate *Bone Miner.* **25** 123–34

Eichert D, Drouet C, Sfihi H, Rey C and Combes C 2009 Nanocrystalline apatite-based biomaterials: synthesis, processing and characterization *Biomaterials Research Advences* ed J B Kendall (Hauppange, NY: Nova Science)

Eichert D, Sfihi H, Combes C and Rey C 2004 Specific characteristics of wet nanocrystalline apatites. Consequences on biomaterials and bone tissue *Key Eng. Mater.* **254** 927–30

Elliott S N, Mcknight W, Davies N M, Macnaughton W K and Wallace J L 1997 Alendronate induces gastric injury and delays ulcer healing in rodents *Life Sci.* **62** 77–91

Eriksen E F, Eghbali Fatourechi G Z and Khosla S 2007 Remodeling and vascular spaces in bone *J. Bone Miner. Res.* **22** 1–6

Errassifi F 2011 Mécanismes d'adsorption du risédronate par des phosphates de calcium biologiques: applications aux biomatériaux *PhD Thesis* University Cadi Ayyad Marrakech, Morocco http://tel.archives.ouvertes.fr/tel-00667418

Errassifi F *et al* 2010 Adsorption on apatitic calcium phosphates: application to drug delivery *Advances in Bioceramics and Biotechnologies. Ceramic Transactions* ed R Narayan and J Mckittrick (New Jersey: The American Ceramic Society) pp 159–74

Errassifi F, Sarda S, Barroug A, Lebugle A, Legrouri A, Sfihi H and Rey C 2009 Adsorption of a bisphosphonate onto apatitic calcium phosphates: role of surface characteristics *Recherphos: Proc. Covaphos III (Marrakech Morocco, 18–20 March 2009)* pp 153–9

Fleisch H 2000 *Bisphosphonates in Bone Disease: From the Laboratory to the Patient* (New York: Academic)

Fromigue O and Body J 2002 Bisphosphonates influence the proliferation and the maturation of normal human osteoblasts *J. Endocrinol. Invest.* **25** 539

Grossmann G, Grossmann A, Ohms G, Breuer E, Chen R, Golomb G, Cohen H, Hägele G and Classen R 2000 Solid-state NMR of bisphosphonates adsorbed on hydroxyapatite *Magn. Reson. Chem.* **38** 11–6

Hoffman A, Stepensky D, Ezra A, Van Gelder J M and Golomb G 2001 Mode of administration-dependent pharmacokinetics of bisphosphonates and bioavailability determination *Int. J. Pharm.* **220** 1–11

Im G I, Qureshi S A, Kenney J, Rubash H E and Shanbhag A S 2004 Osteoblast proliferation and maturation by bisphosphonates *Biomaterials* **25** 4105–15

Josse S *et al* 2005 Novel biomaterials for bisphosphonate delivery *Biomaterials* **26** 2073–80

Juillard A, Falgayrac G, Cortet B, Vieillard M-H, Azaroual N, Hornez J-C and Penel G 2010 Molecular interactions between zoledronic acid and bone: an *in vitro* Raman microspectroscopic study *Bone* **47** 895–904

Kos M and Luczak K 2009 Bisphosphonates promote jaw osteonecrosis through facilitating bacterial colonisation *Biosci. Hypotheses* **2** 34–6

Langmuir I 1918 The adsorption of gases on plane surfaces of glass, mica and platinum *J. Am. Chem. Soc.* **40** 1361–403

Leu C-T, Luegmayr E, Freedman L P, Rodan G A and Reszka a A 2006 Relative binding affinities of bisphosphonates for human bone and relationship to antiresorptive efficacy *Bone* **38** 628–36

Mcleod K, Anderson G I, Dutta N K, Smart R S, Voelcker N H, Sekel R and Kumar S 2006 Adsorption of bisphosphonate onto hydroxyapatite using a novel co-precipitation technique for bone growth enhancement *J. Biomed. Mater. Res.* A **79** 271–81

Meunier P J 2005 Introduction: les défis épidémiologiques et thérapeutiques de l'ostéoporose *Rev. Rhum.* **72** S1–3

Mönkkönen J, Similä J and Rogers M J 1998 Effects of tiludronate and ibandronate on the secretion of proinflammatory cytokines and nitric oxide from macrophages *in vitro Life Sci.* **62** 95–102

Montel G, Bonel G, Heughebaert J C, Trombe J C and Rey C 1981 New concepts in the composition, crystallization and growth of the mineral component of calcified tissues *J. Cryst. Growth* **53** 74–99

Mosmann T 1983 Rapid colorimetric assay for cellular growth and survival: application to proliferation and cytotoxicity assays *J. Immunol. Methods* **65** 55–63

Mukherjee S, Song Y and Oldfield E 2008 NMR investigations of the static and dynamic structures of bisphosphonates on human bone: a molecular model *J. Am. Chem. Soc.* **130** 1264–73

Nancollas G H, Tang R, Phipps R J, Henneman Z, Gulde S, Wu W, Mangood A, Russell R G and Ebetino F H 2006 Novel insights into actions of bisphosphonates on bone: differences in interactions with hydroxyapatite *Bone* **38** 617–27

Ouizat S, Barroug A, Legrouri A and Rey C 1999 Adsorption of bovine serum albumin on poorly crystalline apatite: influence of maturation *Mater. Res. Bull.* **34** 2279–89

Palazzo B, Iafisco M, Laforgia M, Margiotta N, Natile G, Bianchi C L, Walsh D, Mann S and Roveri N 2007 Biomimetic hydroxyapatite-drug nanocrystals as potential bone substitutes with antitumor drug delivery properties *Adv. Funct. Mater.* **17** 2180–8

Panzavolta S, Torricelli P, Bracci B, Fini M and Bigi A 2009 Alendronate and Pamidronate calcium phosphate bone cements: setting properties and *in vitro* response of osteoblast and osteoclast cells *J. Inorg. Biochem.* **103** 101–6

Penel G, Leroy G, Rey C and Bres E 1998 MicroRaman spectral study of the PO_4 and CO_3 vibrational modes in synthetic and biological apatites *Calcif. Tissue Int.* **63** 475–81

Rey C, Collins B, Goehl T, Dickson I R and Glimcher M J 1989 The carbonate environment in bone mineral: a resolution-enhanced Fourier transform infrared spectroscopy study *Calcif. Tissue Int.* **45** 157–64

Rey C, Combes C, Drouet C, Lebugle A, Sfihi H and Barroug A 2007a Nanocrystalline apatites in biological systems: characterisation, structure and properties *Mater. Wiss. Werkst.tech.* **38** 996–1002

Rey C, Combes C, Drouet C, Sfihi H and Barroug A 2007b Physico-chemical properties of nanocrystalline apatites: implications for biominerals and biomaterials *Mater. Sci. Eng.* C **27** 198–205

Rey C, Hina A, Tofighi A and Glimcher M J 1995 Maturation of poorly crystalline apatites: chemical and structural aspects *in vivo* and *in vitro Cells Mater.* **5** 345–56

Rodan G A and Fleisch H A 1996 Bisphosphonates: mechanisms of action *J. Clin. Invest.* **97** 2692

Roussière H *et al* 2008 Reaction of zoledronate with β-tricalcium phosphate for the design of potential drug device combined systems *Chem. Mater.* **20** 182–91

Russell R G and Rogers M J 1999 Bisphosphonates: from the laboratory to the clinic and back again *Bone* **25** 97–106

Russell R G, Watts N B, Ebetino F H and Rogers M J 2008 Mechanisms of action of bisphosphonates: similarities and differences and their potential influence on clinical efficacy *Osteoporos. Int.* **19** 733–59

Scherrer P 1918 Bestimmung der Grösse und der inneren Struktur von Kolloidteilchen mittels Röntgenstrahlen *Nachr. Ges. Wiss. Gött.* **26** 98–100

Vilamitjana-Amedee J, Bareille R, Rouais F, Caplan A I and Harmand M F 1993 Human bone marrow stromal cells express an osteoblastic phenotype in culture *In Vitro Cell. Dev. Biol. Anim.* **29** 699–707

Von Knoch F, Jaquiery C, Kowalsky M, Schaeren S, Alabre C, Martin I, Rubash H E and Shanbhag A S 2005 Effects of bisphosphonates on proliferation and osteoblast differentiation of human bone marrow stromal cells *Biomaterials* **26** 6941–9

Wood R 1930 Raman spectra of benzene and diphenyl *Phys. Rev.* **36** 1431

Wood R and Collins G 1932 Raman spectra of a series of normal alcohols and other compounds *Phys. Rev.* **42** 386